Journal of Power Sources 318 (2016) 170–177

Contents lists available at ScienceDirect

Journal of Power Sources

journal homepage: www.elsevier.com/locate/jpowsour

Enhanced charging capability of lithium metal batteries based on lithium bis(trifluoromethanesulfonyl)imide-lithium bis(oxalato) borate dual-salt electrolytes

Hongfa Xiang [a, b], Pengcheng Shi [b], Priyanka Bhattacharya [a], Xilin Chen [a], Donghai Mei [c], Mark E. Bowden [d], Jianming Zheng [a], Ji-Guang Zhang [a], Wu Xu [a, *]

[a] Energy and Environment Directorate, Pacific Northwest National Laboratory, Richland, WA 99354, USA
[b] School of Materials Science and Engineering, Hefei University of Technology, Hefei, Anhui 230009, China
[c] Physical and Computational Sciences Directorate, Pacific Northwest National Laboratory, Richland, WA 99354, USA
[d] Environmental and Molecular Sciences Laboratory, Pacific Northwest National Laboratory, Richland, WA 99354, USA

HIGHLIGHTS

- Fast chargeability of Li metal batteries with carbonate electrolytes was studied.
- LiTFSI-LiBOB electrolyte greatly enhances fast chargeability of Li metal battery.
- LiTFSI-LiBOB electrolyte gives much longer cycle life than $LiPF_6$ electrolyte.
- LiTFSI-LiBOB electrolyte builds up a thinner interphase layer on Li metal anode.
- LiTFSI-LiBOB electrolyte leads to more conductive sulfur-rich interphase layer.

GRAPHICAL ABSTRACT

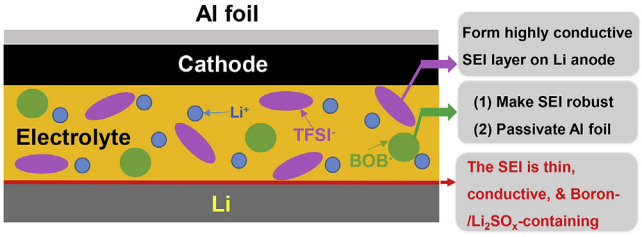

ARTICLE INFO

Article history:
Received 6 February 2016
Received in revised form
31 March 2016
Accepted 4 April 2016

Keywords:
Lithium metal battery
Dual-salt electrolyte
Lithium metal protection
Fast chargeability
Charge current density
Cycling stability

ABSTRACT

Rechargeable lithium (Li) metal batteries with conventional $LiPF_6$-carbonate electrolytes have been reported to fail quickly at charging current densities of about 1.0 mA cm^{-2} and above. In this work, we demonstrate the rapid charging capability of Li||$LiNi_{0.8}Co_{0.15}Al_{0.05}O_2$ (NCA) cells can be enabled by a dual-salt electrolyte of lithium bis(trifluoromethanesulfonyl)imide (LiTFSI) and lithium bis(oxalato)borate (LiBOB) in a carbonate solvent mixture. The cells using the LiTFSI-LiBOB dual-salt electrolyte significantly outperform those using the $LiPF_6$ electrolyte at high charging current densities. At the charging current density of 1.50 mA cm^{-2}, the Li||NCA cells with the dual-salt electrolyte can still deliver a discharge capacity of 131 mAh g^{-1} and a capacity retention of 80% after 100 cycles. The Li||NCA cells with the $LiPF_6$ electrolyte start to show fast capacity fading after the 30th cycle and only exhibit a low capacity of 25 mAh g^{-1} and a low retention of 15% after 100 cycles. The reasons for the good chargeability and cycling stability of the cells using the LiTFSI-LiBOB dual-salt electrolyte can be attributed to the good film-formation ability of the electrolyte on the Li metal anode and the highly conductive nature of the sulfur-rich interphase layer.

* Corresponding author.
E-mail address: wu.xu@pnnl.gov (W. Xu).

http://dx.doi.org/10.1016/j.jpowsour.2016.04.017
0378-7753/

1. Introduction

Continuous development of portable electronics, electric vehicles, and the smart grid requires energy storage systems that have an energy density that is higher than the state-of-the-art lithium (Li)-ion batteries (LIBs). To this end, Li metal batteries (LMBs) are considered the "holy grail" of energy storage systems because of Li metal's extremely high theoretical specific capacity (3860 mAh g^{-1}) and the lowest redox potential (−3.040 V vs. standard hydrogen electrode) [1]. The Li metal anode is superior in specific energy to the conventional graphite anode (whose theoretical specific capacity is only 372 mAh g^{-1}) used in LIBs [2]. Therefore, Li metal has been widely used for the anodes in Li-sulfur batteries [3,4] and Li-air batteries [5,6]. Compared to the problematical sulfur or air cathodes, LMBs using intercalation compounds widely used in LIBs or high-voltage conversion compounds as cathode materials could be more promising in meeting the increasing need for electrochemical energy storage systems that have high energy densities [7]. As reported by Gallagher et al., recently, the LMBs with Li metal anodes and Li-rich layered oxide cathodes have a theoretical energy density of ca. 900 Wh Kg^{-1}, which is twice that of the graphite anode and $LiNi_{1/3}Co_{1/3}Mn_{1/3}O_2$ cathode (ca. 400 Wh Kg^{-1}) [8].

Efforts to develop LMBs before the 1980s proved fruitless mainly because of the safety issues induced by the growth of Li dendrites during repeated charge/discharge cycles [8–11]. Recently, technologies that suppress the growth of Li dendrites have been widely investigated and developed; e.g., use of polymer or solid-state electrolytes [12,13], highly concentrated electrolytes [14–16], self-healing electrostatic shield electrolyte additives [17,18], and protective layers coated on Li metal anodes [19,20]. It should be noted that the cycling stability of Li metal anodes with high Coulombic efficiency and capacity retention, especially at relatively high charge/discharge current densities, needs to be guaranteed in advance to ensure successful commercialization of LMBs. Lv et al. reported that in Li||$LiNi_{0.8}Co_{0.15}Al_{0.05}O_2$ (NCA) cells with the conventional $LiPF_6$-carbonate-based electrolyte, fast capacity fading was observed during charging at high current densities due to the quick formation of a highly resistive solid electrolyte interphase (SEI) entangled with "dead" Li metal particles [21]. In Li||$LiCoO_2$ cells, the ionic liquid (IL)-based electrolyte containing a high concentration of 3.2 mol kg^{-1} lithium bis(fluorosulfonyl)imide [LiFSI, $LiN(SO_2F)_2$] in *N*-propyl-*N*-methylpyrrolidinium bis(fluorosulfonyl) imide exhibited excellent rate capability, in spite of its significantly higher viscosity and lower conductivity [22].

Compared to the use of high-cost ILs, the reformulation of electrolytes with different Li salts is an easy and cost-effective approach. Recently, Miao et al. explored a dual-salt electrolyte composed of LiFSI and lithium bis(trifuoromethanesulfonyl)imide [LiTFSI, $LiN(SO_2CF_3)_2$] in mixed ether solvents in order to simultaneously cope with the low cycle efficiency and Li dendrite formation on the Li metal anode during charge/discharge processes [23]. Our team also investigated the effects of the highly concentrated electrolytes of LiFSI or LiTFSI in ethers on improving Li Coulombic efficiency (CE) and suppressing the growth of Li dendrites [14]. With the unique protection of SEI films and the improved Li growth pattern, a high CE of ca. 99% and dendrite-free Li deposition have been achieved. Moreover, the excellent cycling performance and favorable Li morphology can be retained even at a high current density of 10 mA cm^{-2}. However, the ether-based electrolytes normally are not electrochemically stable at voltages around 4 V, so they cannot be used in batteries that need to be charged to 4 V and above.

Basically, it is more practical to reformulate electrolytes based on the state-of-the-art $LiPF_6$-carbonate electrolytes to meet the requirements for LMBs with high-voltage intercalation or conversion cathode materials and at high current densities during cycling. Compared to $LiPF_6$, which is sensitive to moisture and heat, LiTFSI is thermally stable and insensitive to moisture [24,25]. Xu stated an empirical rule concerning the resistance of the SEI on the Li metal anode: an electrolyte with higher bulk ion conductivity usually results in an SEI of lower impedance [24]. Fast charging of LMBs using the LiTFSI-based electrolytes may be enabled by the highly conductive SEI formed on the Li electrode. The main limitation of LiTFSI is its corrosion of the aluminum (Al) current collector at voltages above 3.7 V [26–28]. Recently, we reported the effects of the dual salts of LiTFSI and lithium bis(oxalato)borate [LiBOB, $LiB(C_2O_4)_2$] on the suppression of Al corrosion and the improvement in cell performance of a Li||$LiFePO_4$ (LFP) battery system with a low LFP loading [29]. In this work, the effects of LiTFSI-LiBOB dual-salt electrolytes on the charge rate of LMBs with a relatively high loading NCA electrode are reported.

2. Experimental

LiTFSI, $LiPF_6$, ethylene carbonate (EC), ethyl methyl carbonate (EMC), and dimethyl carbonate (DMC) of battery grade were ordered from BASF Battery Materials. LiBOB of battery grade was obtained from Chemetall with no charge. All of the chemicals were stored in an MBraun glove box filled with purified argon for the preparation of electrolytes. The dual-salt electrolyte was composed of 0.6 M LiTFSI and 0.4 M LiBOB (or $LiTFSI_{0.6}$-$LiBOB_{0.4}$) in EC-EMC (4:6 by wt.). For comparison, the control electrolyte composed of 1.0 M $LiPF_6$ in the same EC-EMC (4:6 by wt.) mixture also was investigated. Coated graphite (MAG-10, 1.53 mAh cm^{-2}) and NCA (1.50 mAh cm^{-2}) electrodes were provided by the Argonne National Laboratory CAMP Facility. The graphite anode contained 92 wt% MAG-10 graphite with 8 wt% Kureha #C binder, and the NCA cathode consisted of 86 wt% Toda NCA, 4 wt% SFG-6 conductive additive, 2 wt% Super P Li, and 8 wt% Solvay 5130 binder. More details can be found in our recent paper [30]. High-purity Li chips (15.6 mm in diameter and 0.45 mm in thickness) were purchased from MTI Corporation. 2325-type coin cell kits were ordered from National Research Council of Canada.

Li||NCA coin cells with 80 μL electrolyte were assembled in the MBraun glove box to evaluate the electrochemical properties of various electrolytes. All cells were tested by undergoing galvanostatic charge/discharge cycles on an Arbin BT-2000 battery testing station at room temperature using various current densities in the voltage range of 3.0–4.3 V. A current density rate of 1C (i.e., charge or discharge in 1 h) was set to 1.5 mA cm^{-2}. Formation cycles were initially conducted for two cycles at 0.1C rate for both charging and discharging. These cycles were then followed by further cycling at various C rates. To understand the mechanism of the cycling failure, some of the cycled cells were disassembled to harvest the Li metal anodes. Electrochemical impedance spectra (EIS) analysis was performed on a Solartron 1287 electrochemical workstation coupled with a Solartron 1255B frequency response analyzer with a 10 mV perturbation at open circuit potential in the frequency range of 10^6–10^{-1} Hz.

Cycled Li anodes were obtained from the tested cells for various characterizations. Before the measurements, the Li electrodes were immersed in anhydrous DMC for 24 h and then rinsed with fresh DMC five times to remove the Li salts before drying under vacuum. Scanning electron microscopy (SEM) images and the corresponding energy dispersive X-ray spectroscopy (EDS) analysis of the Li electrodes for both the surface and the cross-section views were conducted on a JEOL 5800 microscope with an Oxford EDS. To avoid electrode contamination or side reactions with atmospheric moisture and oxygen, the samples were transferred in sealed vessels filled with argon. X-ray photoelectron spectroscopy (XPS)

analysis was carried out using an America Thermo ESCALAB250 instrument. Fourier transform infrared spectrometer (FTIR) spectra were collected from 4000 cm^{-1} to 500 cm^{-1} on a Nicolet-670 FTIR spectrometer.

The density functional theory (DFT) method was employed to calculate the lowest unoccupied molecular orbital (LUMO) energies of the Li salts and solvents as implemented in the Gaussian 09 program suite [31]. The B3LYP functional combined with the 6–311++G(d,p) basis set was chosen in geometry optimization calculations [32,33].

3. Results and discussion

Firstly, in order to evaluate the fast-charging properties of the NCA electrode, the cycling performances of the graphite||NCA cells and the Li||NCA cells with the conventional $LiPF_6$/EC-EMC electrolyte at 1.50 mA cm^{-2} (equal to 1C charge rate) were tested and compared. Prior to the 1C cycling, all cells were conditioned through two formation cycles to allow the SEI layers to be generated on both the anodes and cathodes: the Li||NCA cells were charged and discharged at 0.15 mA cm^{-2} (i.e., 0.1C rate) in the voltage range from 3.0 V to 4.3 V vs. Li/Li^+, while the graphite||NCA cells were charged and discharged at 0.075 mA cm^{-2} (i.e., 0.05C rate) between 3.0 V and 4.3 V. As shown in Fig. 1a, the LMB (i.e., Li||NCA cell) is clearly demonstrated to have a higher capacity than the LIB (i.e., graphite||NCA cell) before the former experiences a huge capacity fading.

The NCA cathode used in this work had an NCA mass loading of 10.2 mg cm^{-2}, which is an intermediate mass loading compared to those used in commercial LIBs. A thicker electrode means a higher capacity of the total cell, so more Li is de-intercalated from and intercalated into the cathode, and more Li is deposited on and stripped from the Li anode, where the electrochemical performance of the Li metal cells and the morphology change of the Li metal anode are quite different from the cells with thin electrodes with just 1–2 mg active material.

As shown in Fig. 1a, the graphite||NCA cell with a conventional $LiPF_6$/EC-EMC electrolyte exhibits excellent cycling stability at 1.50 mA cm^{-2}, indicating that the Li^+ ion extraction from and insertion into the NCA cathode material work fine at the 1C rate and the NCA electrode is quite stable at this current density. However, the Li||NCA cell with the same conventional $LiPF_6$/EC-EMC electrolyte experiences a continuous capacity fading and even a sharp capacity drop after 30 cycles at the same current density of 1.50 mA cm^{-2} for charge and discharge. Therefore, the Li metal anode should be responsible for the fast capacity fading of the Li||NCA cell at the 1C rate of cycling.

Furthermore, the cycling performances of the Li||NCA cells with the conventional $LiPF_6$/EC-EMC electrolyte at various charge rates and at the 1C discharge rate were tested and the results are shown in Fig. 1b. At low charge current densities (0.30 and 0.75 mA cm^{-2}), the Li||NCA cells exhibit good cycling stability, even though the cell at 0.75 mA cm^{-2} has a slightly lower capacity retention after 100 cycles than that at 0.30 mA cm^{-2}. In addition, both cells always keep high cycling efficiency above 98% after two formation cycles. However, when the charge current density is increased to 1.50 mA cm^{-2}, a huge capacity fading appears after ~30 cycles, and the cycling efficiency drops to ~90%. Furthermore, at the current density of 3.00 mA cm^{-2}, the fast capacity fading starts after 20 cycles and the cycling efficiency drops similarly. This variation in the cycling efficiency curve seems to be an indicator of fast capacity fading. The capacity fading trend with charge current density is similar to what Lv et al. reported [21], and is mainly caused by the impedance increase.

It is well known that LiBOB has the advantage in SEI film formation over the commonly used $LiPF_6$ in LIBs, but its low solubility in carbonate solvents cannot meet the requirement for high conductivity of the electrolytes, especially for high-power applications [34,35]. LiTFSI has advantages over $LiPF_6$ in good thermal stability and insensitivity toward moisture, and the LiTFSI-electrolytes have high Li^+-ion conductivities similar to the $LiPF_6$-based electrolytes. However, LiTFSI causes serious corrosion of the Al current collector due to the formation of soluble $Al(TFSI)_3$ [27,36]. Recently, we found that dual-salt LiTFSI-LiBOB electrolytes exhibit good integrated performance, such as excellent stability, no corrosion of Al, and high Li^+-ion conductivity, so that this kind of dual-salt electrolyte is a promising alternative to $LiPF_6$ [29]. In previous work [29], it was reported that an Al current collector has excellent compatibility with the $LiTFSI_{0.6}$-$LiBOB_{0.4}$/EC-EMC (4:6 by wt.) electrolyte up to 3.9 V vs. Li/Li^+. Therefore, prior to this electrolyte being used in Li||NCA cells, the stability of the Al current collector in this dual-salt electrolyte was first investigated at 4.3 V. As shown in Fig. S1 (in the Supporting Information), after the Li||Al cells with the dual-salt electrolyte were charged to 4.3 V and held at this voltage at 60 °C for 7 days, the Al foil still remained intact and no signs of corrosion were observed, demonstrating that the Al current collector is stable with this LiTFSI-LiBOB dual-salt electrolyte at 4.3 V.

Fig. 2 shows the cell performance of the dual-salt LiTFSI-LiBOB electrolyte in Li||NCA cells compared to that of the conventional $LiPF_6$ electrolyte. In Fig. 2a, the cell with the dual-salt electrolyte

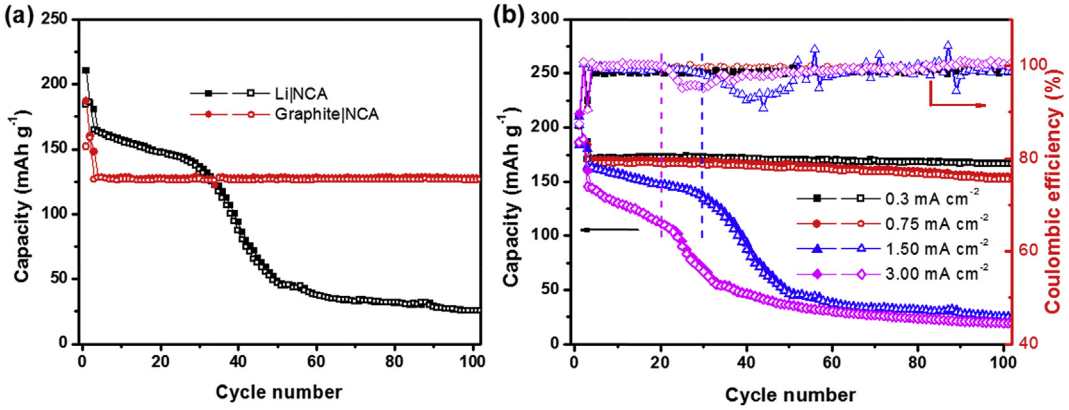

Fig. 1. (a) Cycling performance of graphite||NCA cells and Li||NCA cells with the electrolyte of 1 M $LiPF_6$/EC-EMC (4:6 by wt.) at 1.50 mA cm^{-2} current density. (b) Cycling stability of capacity and cycling efficiency of Li||NCA cells charged at various current densities and discharged at 1.50 mA cm^{-2}. Prior to cycling, all cells were conditioned with two formation cycles at a current density of 0.15 mA cm^{-2} for Li||NCA cells and 0.075 mA cm^{-2} for graphite||NCA cells in the voltage range of 3.0–4.3 V.

exhibits a slightly higher reversible capacity (189 mAh g^{-1}) and initial cycling efficiency (88.7%) than that using the $LiPF_6$ electrolyte (with a capacity of 183 mAh g^{-1} and cycling efficiency of 86.7%). This result at least further proves that the dual-salt LiTFSI-LiBOB electrolyte causes no Al corrosion. Furthermore, the results of cycling performance in Fig. 2b show that the Li||NCA cell with the dual-salt LiTFSI-LiBOB electrolyte has much better cycling stability than those with the $LiPF_6$ electrolyte at 1.50 mA cm^{-2} for both charge and discharge. After 100 cycles, the cell with the dual-salt electrolyte can still deliver a discharge capacity of 131 mAh g^{-1} (80% retention compared to the first discharge capacity at the 1C rate after two formation cycles at C/10), while that with the $LiPF_6$ electrolyte only exhibits a low capacity of 25 mAh g^{-1} (15% retention). In terms of cycling efficiency, the cell with the dual-salt electrolyte always maintains a stable high level of 97.5% after the two formation cycles, which is slightly lower than that achieved with the $LiPF_6$ electrolyte (close to 99% but with large fluctuations). The reason is probably related to the instability of LiBOB at the NCA cathode surface at 4.3 V [10,24], but more investigation is needed to confirm this to be true.

Fig. 2c and d shows the voltage profiles of the different cycles for the cells using the LiTFSI-LiBOB and $LiPF_6$ electrolytes, respectively. Clearly, the capacity fading of the cell with the dual-salt electrolyte is quite slow and the voltage change is not remarkable (Fig. 2c). However, the cell with the $LiPF_6$ electrolyte exhibits a fast capacity decay with increasing cycle number, along with a huge voltage plateau change between the 20th and 50th cycles (Fig. 2d). The evolution of the voltage profiles of the cell with the $LiPF_6$ electrolyte during the period from the 30th to 45th cycles is shown in Fig. 2e, which more clearly indicates the fast capacity drop. The charge voltage profiles experience a huge change (from concave to bulged), which suggests there is a charge mechanism change in the LMBs for the $LiPF_6$ electrolyte. Herein, the voltage difference (ΔV) between the midpoint of the charge curve and that of the corresponding discharge curve is used as an indicator of polarization, and the voltage difference with cycling of the two electrolytes is

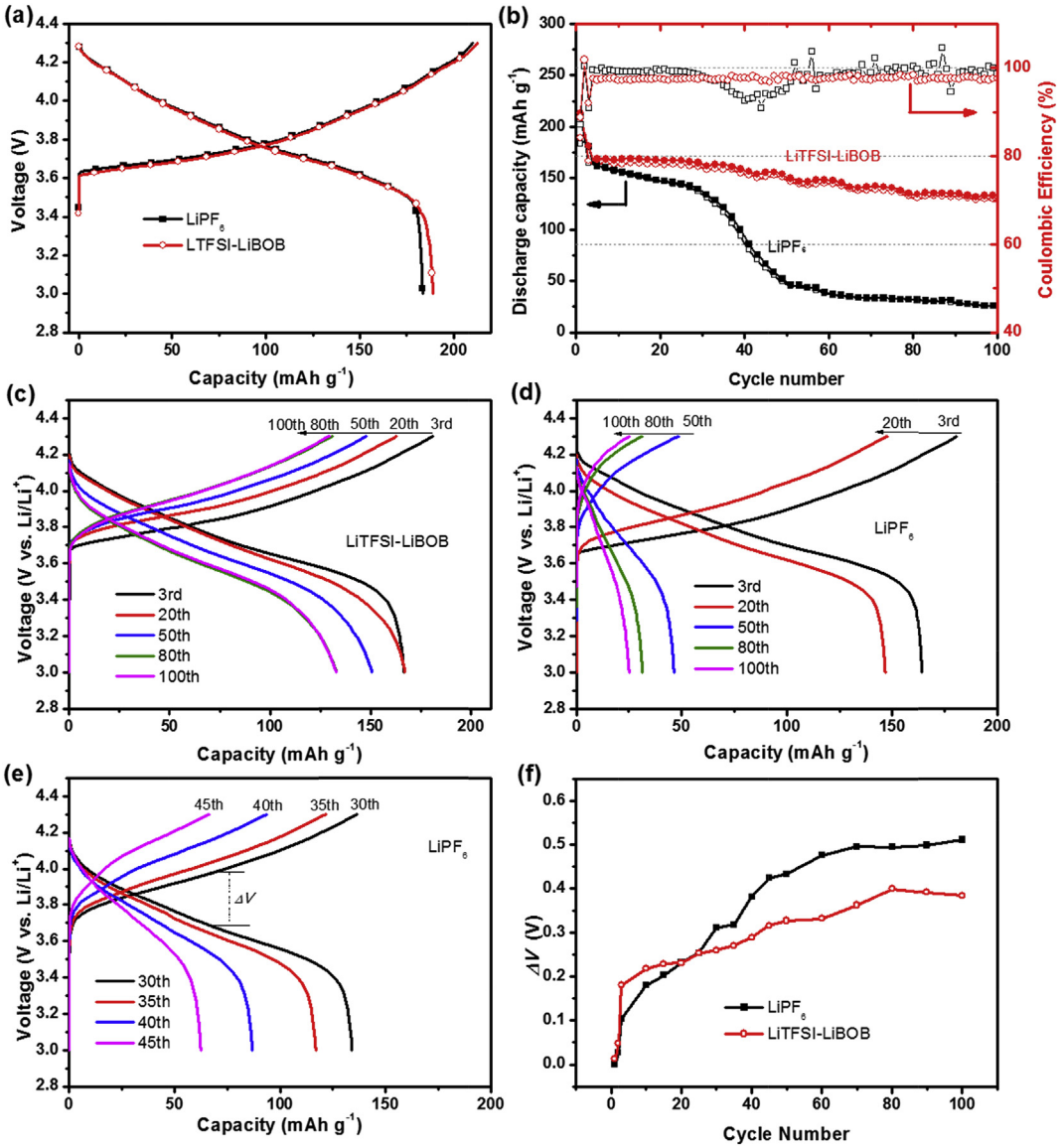

Fig. 2. Initial voltage profiles (a) and cycling performance (b) of the Li||NCA cells using the $LiPF_6$ and LiTFSI-LiBOB electrolytes. Charge-discharge curves of the Li||NCA cells using the LiTFSI-LiBOB electrolyte (c) and the $LiPF_6$ electrolyte (d,e) and the voltage differences ΔV (f) between the midpoint of the charge curve and that of the corresponding discharge curve at different cycles.

compared in Fig. 2f. Obviously, the polarization of the Li||NCA cell using either electrolyte continues to increase with increasing cycle number, but the LiTFSI-LiBOB dual-salt electrolyte has a slower rise and remains at a lower level than the $LiPF_6$ electrolyte after 20 cycles, indicating that the interphase formed in the LiTFSI-LiBOB electrolyte is more conductive for Li^+ ions than that in $LiPF_6$ electrolyte. These electrochemical performance results strongly suggest that the dual-salt electrolyte allows the Li metal electrode to have good stability and tolerance for fast charging.

EIS has been used to reveal the ionic conductivity of the interphase films on Li metal anodes formed in the two electrolytes studied in this work. Fig. 3 shows the Nyquist plots of the Li||NCA cells with the $LiPF_6$ (a) and the LiTFSI-LiBOB (b) electrolytes at the 2nd (i.e., right after the two formation cycles) and the 100th cycles. All Nyquist plot curves except for the one for the cell with $LiPF_6$ electrolyte at the 100th cycle (Fig. 3a) are composed of two deformed or incomplete semicircles in the high-to-medium frequency range and a short inclined line in the low frequency range. The semicircle in the high frequency range can be ascribed to Li^+ ion migration through the interphase film between electrode and electrolyte, while the semicircle in the medium frequency range is assigned to the charge transfer process. However, the Nyquist plot for the cell with $LiPF_6$ electrolyte at the 100th cycle exhibits only one semicircle in the high frequency range, which can be associated with surface film resistance, but the semicircle for the charge transfer does not show up. All cells show reduced SEI resistances after 100 cycles when compared to those after two formation cycles, especially for the cell with the dual-salt electrolyte. This is probably because the SEI films after cycling have high surface areas (see Fig. S2) and contain lots of fine "inactive" Li particles (Fig. S3). Although the Li||NCA cell with the dual-salt electrolyte exhibits higher SEI impedance than that of the $LiPF_6$ electrolyte right after the two formation cycles, the former definitely shows lower surface film resistance than the latter after cycling. This suggests that the interphase formed on the Li electrode in the LiTFSI-LiBOB electrolyte is more conductive for Li^+ ions than that in $LiPF_6$ electrolyte.

The intercept impedance on the Z-real axis at high frequency in the Nyquist plots reflects the resistance (R_b) of the bulk electrolyte solution. The bulk resistance from the $LiPF_6$ electrolyte distinctly increased after 100 cycles, as shown in Fig. 3a, indicating the consumption of this electrolyte during long cycling. However, the bulk resistance from the dual-salt electrolyte remained quite stable (Fig. 3b), suggesting that the SEI film from this LiTFSI-LiBOB electrolyte is compact and prevents continuous reactions between the Li metal anode and the electrolyte components. Here, the difference between the surface interphase impedances (R_{sf}) at high frequency is mainly attributed to the change in the SEI interphase on the Li electrode. After 100 cycles, the SEI interface impedance (R_{sf}) from the dual-salt electrolyte (Fig. 3b) is much lower than that from the $LiPF_6$ electrolyte (Fig. 3a), which suggests that the interphase film formed on the Li electrode in the LiTFSI-LiBOB electrolyte is much more conductive for Li^+ ions than that in $LiPF_6$ electrolyte. Although the Nyquist plot for the $LiPF_6$ electrolyte does not exhibit the semicircle for the charge transfer resistance (R_{ct}) after 100 cycles (Fig. 3a), so it is hard to derive the exact value of R_{ct} after 100 cycles, nevertheless, one can deduce that the high R_{ct} value after 2 formation cycles will result in a high R_{ct} value after 100 cycles as well. Therefore, the total resistance of the cell with the $LiPF_6$ electrolyte after 100 cycles will be higher than that with the dual-salt electrolyte, resulting in higher polarization, as shown in Fig. 2f.

To further explore the reasons for the fast chargeability of the LiTFSI-LiBOB dual-salt electrolyte and the rapid decay of the $LiPF_6$ electrolyte, the surfaces of the cycled Li electrodes from the Li||NCA cells after 100 cycles were washed carefully with anhydrous DMC at least 5 times, dried, and investigated using several technologies. Fig. 4 shows the SEM images of the Li metal electrode surfaces after cycling in LiTFSI-LiBOB electrolyte and $LiPF_6$ electrolyte for 100 cycles. It is clearly seen that a thick interphase layer of about 100 μm covered the Li metal electrode cycled in the $LiPF_6$-based electrolyte (Fig. 4a). However, the thickness of the interphase layer on the Li metal electrode cycled in the dual-salt electrolyte is about 20 μm (Fig. 4b), just one-fifth of the interphase layer formed in the $LiPF_6$-based electrolyte. The thin interphase layer from the LiTFSI-LiBOB electrolyte is mainly caused by its ability to form a good film on Li metal.

The EDS results from the cycled Li metal surfaces (Fig. S4) show that a large amount of oxygen (in addition to small amounts of phosphorus, fluorine, and carbon) exists in the interphase of the Li electrode cycled in the $LiPF_6$-based electrolyte. In contrast, large amounts of both oxygen and sulfur (besides trace amounts of carbon and boron) were detected on the Li surface tested in the dual-salt electrolyte. XPS was used to more accurately analyze the chemical components and compositions of the SEI layers formed on the surfaces of the Li electrodes after 100 cycles in the LiTFSI-LiBOB dual-salt and the $LiPF_6$ electrolytes. Fig. S5 shows the wide scans over the whole spectrum range for Li electrodes cycled in the two electrolytes. Both Li electrode surfaces have C 1s, F 1s, O 1s, and Li 1s peaks. However, the SEI layer on the Li electrode cycled in the dual-salt electrolyte also exhibits strong S 2p peak and weak B 1s and N 1s peaks, while that in the $LiPF_6$ electrolyte has only a weak P 2p peak.

When the photoelectron peaks are focused on by running

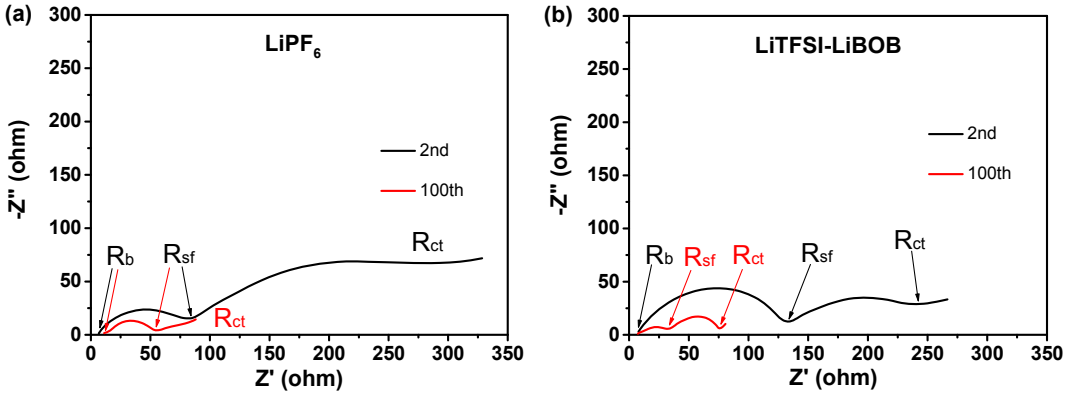

Fig. 3. Nyquist plots of the Li||NCA cells using the $LiPF_6$ electrolyte (a) and the LiTFSI-LiBOB electrolyte (b). All of the tests were carried out after the cells were fully discharged to 3.0 V and then rested for 2 h.

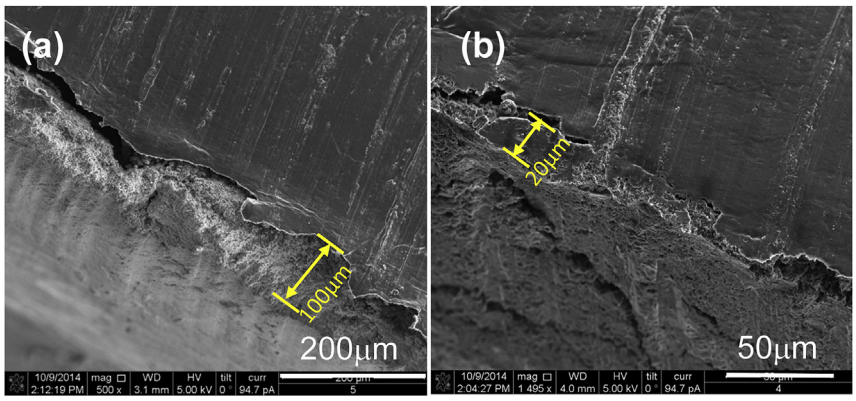

Fig. 4. SEM images of the Li metal electrode surfaces obtained from the Li||NCA cells with the $LiPF_6$ electrolyte (a) and the LiTFSI-LiBOB dual-salt electrolyte (b) after cycling at 1.50 mA cm^{-2} for 100 cycles.

narrow scans, significant differences and more information can be observed. The narrow scan spectra of C 1s, F 1s, O 1s, and Li 1s for the two cycled Li surfaces are compared in Fig. 5a–d, respectively. In the C 1s spectra (Fig. 5a), the sample from the dual-salt electrolyte shows major peaks at 293.1, 289.0, 286.8, and 284.8 eV, as well as a shoulder peak at 290.2 eV, while the Li surface from the $LiPF_6$ electrolyte contains the main peaks at 290.3, 286.8, and 284.8 eV, as well as a minor peak at 289.0 eV. The 293.1 eV peak is for the C–F bond in the $-CF_3$ group, which originates from the $TFSI^-$ anions. The 290.3 eV peak can be ascribed to the C=O in the CO_3 of Li_2CO_3 and/or lithium alkyl carbonate, which are from the decomposition of the carbonate solvents. The peak at 289.0 eV is attributed to the C=O in oxalate [–(O=C)–(C=O)–] compounds [37], which are from the oxalato group in the BOB^- anion. The peaks at 286.8 eV and 284.8 eV are for C–O bond and C–C/C–H bonds, respectively, which originate from organic carbonate solvents as well. The relative intensities of these two peaks (at 286.8 and 284.8 eV) are quite different for the two samples, indicating their different compositions in the formed SEI layers on the two Li electrodes from different electrolytes. Generally, the intensities of the C1s peaks for the Li electrode from the dual-salt electrolyte are much weaker than those from the $LiPF_6$ electrolyte, suggesting that the decompositions of the solvents and salt anions from the dual-salt electrolyte are less than those from the $LiPF_6$ electrolyte, which is also indicated by the fact that the SEI layer from the dual-salt electrolyte is more compact, so the further reactions between Li metal and the electrolytes can be suppressed easily.

In the F 1s spectra (Fig. 5b), the peak at 689.0 eV in the sample from the dual-salt electrolyte is ascribed to the C–F bond of the $-CF_3$ group in the $TFSI^-$ anion, while the peak at 687.0 eV in the

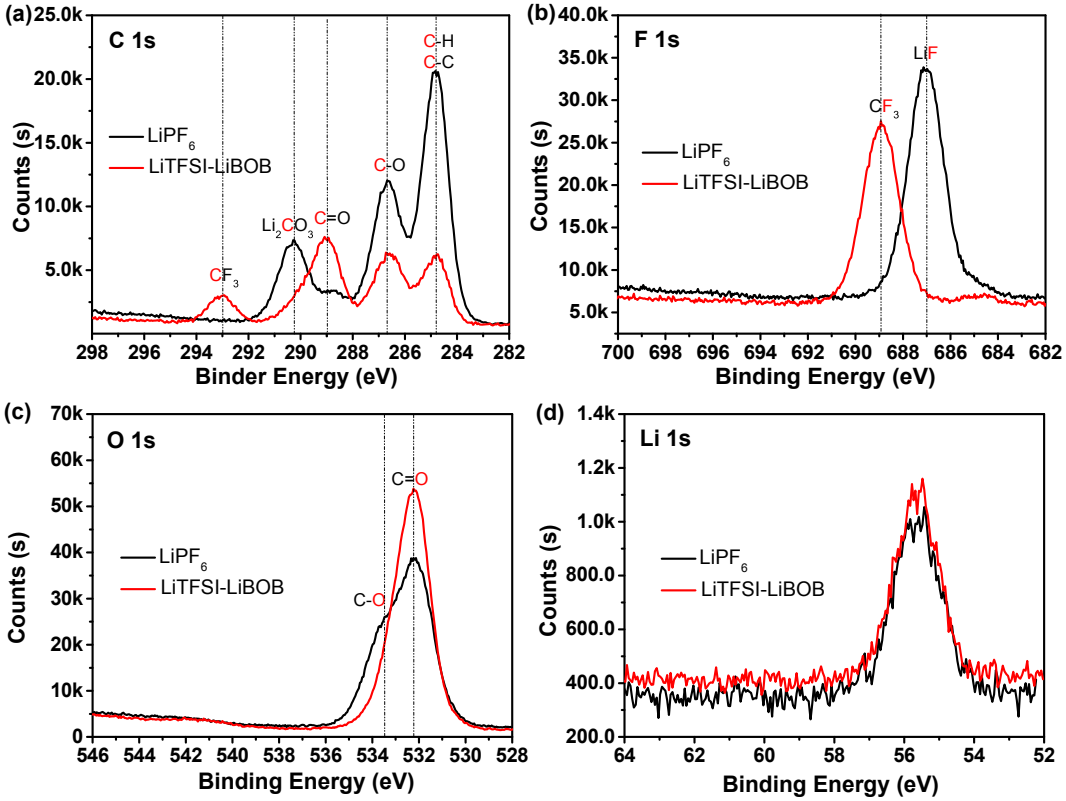

Fig. 5. XPS patterns of Li electrodes after 100 cycles in LiTFSI-LiBOB and $LiPF_6$ electrolytes. (a) C 1s, (b) F 1s, (c) O 1s, and (d) Li 1s.

sample from the $LiPF_6$ electrolyte is for LiF, which is from the decomposition of the PF_6^- anion. In the O 1s spectra (Fig. 5c), the Li sample from the dual-salt electrolyte has a major peak located at 532.2 eV and a small shoulder peak at 533.5 eV, the former belonging to S═O and C═O groups and the latter to the C–O and/or B–O groups. For the sample from the $LiPF_6$ electrolyte, the peaks at 532.2 and 533.5 eV can only be assigned to C═O and C–O, respectively, which originate from the decompositions of carbonate solvents. There is negligible difference for the two samples on the Li 1s spectra (Fig. 5d).

The SEI layers on the Li electrode cycled after 100 cycles in LiTFSI-LiBOB and $LiPF_6$ electrolytes were further analyzed using FTIR and the spectra are shown in Fig. 6. For the SEI formed in the LiTFSI-LiBOB electrolyte, the symmetric CF_3 stretching mode is located at 1200 cm^{-1}, the symmetric SO_2 stretching mode at 1138 cm^{-1}, and the asymmetric SO_2 stretching mode at 1355 cm^{-1} with a shoulder small peak at 1333 cm^{-1}. The bands related to Li_2CO_3 at 1522, 1443, and 862 cm^{-1} are relatively weak, but they are clearly detectable in the deposit from the $LiPF_6$ electrolyte. In both Li samples from the LiTFSI-LiBOB and the $LiPF_6$ electrolytes, the peaks at 1655, 1310, 1100, and 838 cm^{-1} are attributed to lithium alkyl carbonate ($ROCO_2Li$) and oxalate and boron-containing semicarbonate-like species [37].

In general, the electrochemical reduction potential of a compound is correlated with its LUMO energy, and a lower LUMO energy normally means a higher reduction potential. Therefore, the LUMO energies of the salts and solvents studied in this work were calculated by DFT using the Gaussian 09 program suite, and the results are listed in Table 1. Based on this table, the electrochemically reductive decomposition of the salt and the solvent should follow the order from high to low voltage as LiBOB ≫ LiTFSI > $LiPF_6$ ≫ EC > EMC. Xu et al. reported that LiBOB started the irreversible reduction at about 1.7 V vs. Li/Li^+ [38], and Dahn and coworkers [39] found that an irreversible voltage plateau occurred at around 1.2 V on the carbonaceous electrode surface that corresponded to the decomposition of the EC-based solvents. Based on the XPS and FTIR analyses, it can be seen that the main components of the SEI layer formed in the LiTFSI-LiBOB electrolyte are lithium oxalate, boron-containing semicarbonate-like species, and lithium sulfonate-like species, while Li_2CO_3 and LiF are the main components in the SEI layer formed in the $LiPF_6$ electrolyte. According to Aurbach [40], lithium sulfonates (10^{-7} S cm^{-1}) have much higher ionic conductivity than Li_2CO_3 (10^{-8} S cm^{-1}) and LiF (10^{-8} S cm^{-1}). Therefore, the main reason for the fast chargeability of the LiTFSI-LiBOB electrolyte is possibly the thinner and more conductive SEI layers composed of lithium oxalate, boron-containing semicarbonate-like species, and lithium sulfonates.

Table 1
LUMO energies of Li salts and carbonate solvents by DFT calculations.

Salt or solvent	LUMO energy (eV)
$LiPF_6$	−1.44
LiTFSI	−1.52
LiBOB	−3.05
EC	0.94
EMC	1.21

On the basis of the above results and discussion, we propose two reasons for the fast chargeability of the LiTFSI-LiBOB dual-salt electrolyte in LMBs. As shown in Fig. 7, LiTFSI helps to build up a highly conductive SEI layer on the Li electrode consisting of lithium sulfonates during fast charging, which leads to high Li^+ conduction across the SEI layer, and LiBOB makes the SEI layer on the Li electrode robust and stable during cycling, which suppresses the growth of the SEI layer and thus results in a short diffusion distance. Both factors synergistically enhance the charging rate of LMBs based on LiTFSI-LiBOB dual-salt electrolytes. Additionally, LiBOB also passivates the Al foil (the current collector for the cathode) and prevents the consumption of LiTFSI during battery operation.

4. Conclusions

The fast chargeability of the Li||NCA cells with two carbonate-based electrolytes was systematically investigated. The fast capacity fading in the conventional $LiPF_6$ electrolyte is related to the thick interphase layer with high impedance covered on Li metal during fast charging. However, the LiTFSI-LiBOB dual-salt electrolyte exhibited good cycling stability during fast charging, because of the ability of this electrolyte to form a good film on Li metal and the highly conductive nature of the sulfur-rich interface layer. Even though the exact chemistry of the interphase on Li metal is pending, this LiTFSI-LiBOB dual-salt electrolyte is a promising candidate for replacing the conventional $LiPF_6$ electrolyte in fast-chargeable LMBs.

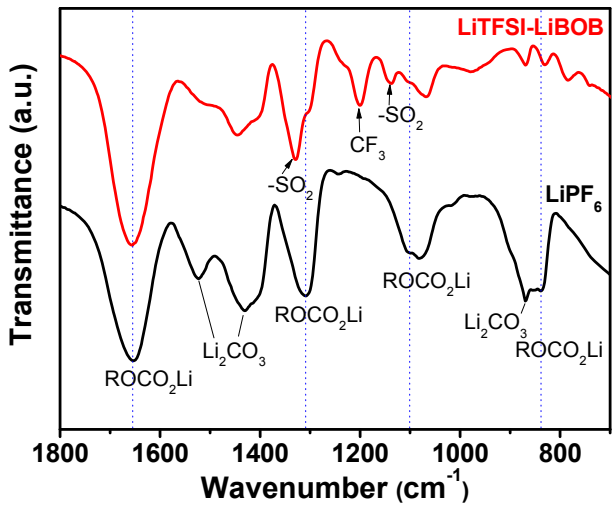

Fig. 6. FTIR spectra of the SEI layers on Li electrodes after 100 cycles in LiTFSI-LiBOB and $LiPF_6$ electrolytes.

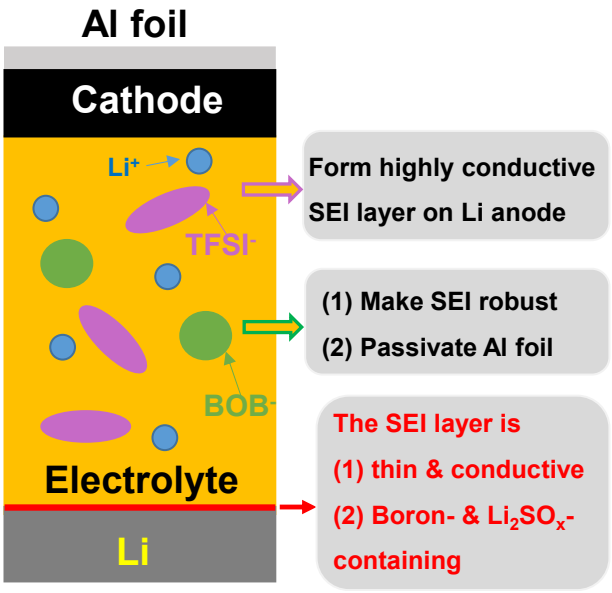

Fig. 7. Schematic illustration of the effects of LiTFSI and LiBOB in the dual-salt electrolyte.

Acknowledgements

This work was supported by the Assistant Secretary for Energy Efficiency and Renewable Energy, Office of Vehicle Technologies, the Advanced Battery Materials Research (BMR) programs of the U.S. Department of Energy (DOE) under Contract No. DE-AC02-05CH11231, Subcontract No. 18769. The microscopic images and spectroscopic measurements were conducted at the William R. Wiley Environmental Molecular Sciences Laboratory (EMSL)—a national scientific user facility located at PNNL, which is sponsored by the DOE's Office of Biological and Environmental Research (BER). H.X. acknowledges the financial support from National Science Foundation of China (Grant No. 51372060). P.B. gratefully acknowledges support from the Linus Pauling distinguished Postdoctoral Fellowship of PNNL. PNNL is operated by Battelle for the DOE under Contract DE-AC05-76RLO1830. The authors thank Mr. Bryant Polzin at ANL for supplying the coated NCA and graphite electrodes. Drs. Jiangfeng Qian, Liang Xiao and Dongping Lv at PNNL are also appreciated for good discussions.

Appendix A. Supplementary data

Supplementary data related to this article can be found at 10.1016/j.jpowsour.2016.04.017.

References

[1] A.I. Bhatt, P. Kao, A.S. Best, A.F. Hollenkamp, Understanding the morphological changes of lithium surfaces during cycling in electrolyte solutions of lithium salts in an ionic liquid, J. Electrochem. Soc. 160 (2013) A1171–A1180.
[2] M. Chiku, W. Tsujiwaki, E. Higuchi, H. Inoue, Determination of the rate-determining step in the electrochemical oxidation of Li metal at the Li negative electrode/Li_2S–P_2S_5 solid electrolyte interface, J. Power Sources 244 (2013) 675–678.
[3] Q. Wang, J. Zheng, E. Walter, H. Pan, D. Lv, P. Zuo, H. Chen, Z.D. Deng, B.Y. Liaw, X. Yu, X. Yang, J.-G. Zhang, J. Liu, J. Xiao, Direct observation of sulfur radicals as reaction media in lithium sulfur batteries, J. Electrochem. Soc. 162 (2015) A474–A478.
[4] X.L. Ji, K.T. Lee, L.F. Nazar, A highly ordered nanostructured carbon-sulphur cathode for lithium-sulphur batteries, Nat. Mater. 8 (2009) 500–506.
[5] G. Girishkumar, B. McCloskey, A.C. Luntz, S. Swanson, W. Wilcke, Lithium - air battery: promise and challenges, J. Phys. Chem. Lett. 1 (2010) 2193–2203.
[6] J.S. Lee, S.T. Kim, R. Cao, N.S. Choi, M. Liu, K.T. Lee, J. Cho, Metal-air batteries with high energy density: Li-air versus Zn-air, Adv. Energy Mater. 1 (2011) 34–50.
[7] M.S. Whittingham, Ultimate limits to intercalation reactions for lithium batteries, Chem. Rev. 114 (2014) 11414–11443.
[8] K.G. Gallagher, S. Goebel, T. Greszler, M. Mathias, W. Oelerich, D. Eroglu, V. Srinivasan, Quantifying the promise of lithium-air batteries for electric vehicles, Energy Environ. Sci. 7 (2014) 1555–1563.
[9] J. Jeong, J.-N. Lee, J.-K. Park, M.-H. Ryou, Y.M. Lee, Stabilizing effect of 2-(triphenylphosphoranylidene) succinic anhydride as electrolyte additive on the lithium metal of lithium metal secondary batteries, Electrochim. Acta 170 (2015) 353–359.
[10] K. Xu, Electrolytes and interphases in Li-ion batteries and beyond, Chem. Rev. 114 (2014) 11503–11618.
[11] W. Xu, J. Wang, F. Ding, X. Chen, E. Nasybulin, Y. Zhang, J.-G. Zhang, Lithium metal anodes for rechargeable batteries, Energy Environ. Sci. 7 (2014) 513–537.
[12] R. Khurana, J.L. Schaefer, L.A. Archer, G.W. Coates, Suppression of lithium dendrite growth using cross-linked polyethylene/poly(ethylene oxide) electrolytes: a new approach for practical lithium-metal polymer batteries, J. Am. Chem. Soc. 136 (2014) 7395–7402.
[13] M. Kotobuki, K. Kanamura, Y. Sato, T. Yoshida, Fabrication of all-solid-state lithium battery with lithium metal anode using Al_2O_3-added $Li_7La_3Zr_2O_{12}$ solid electrolyte, J. Power Sources 196 (2011) 7750–7754.
[14] J. Qian, W.A. Henderson, W. Xu, P. Bhattacharya, M. Engelhard, O. Borodin, J.-G. Zhang, High rate and stable cycling of lithium metal anode, Nat. Commun. 6 (2015) 6362.
[15] S.-K. Jeong, H.-Y. Seo, D.-H. Kim, H.-K. Han, J.-G. Kim, Y.B. Lee, Y. Iriyama, T. Abe, Z. Ogumi, Suppression of dendritic lithium formation by using concentrated electrolyte solutions, Electrochem. Commun. 10 (2008) 635–638.
[16] L. Suo, Y.-S. Hu, H. Li, M. Armand, L. Chen, A new class of solvent-in-salt electrolyte for high-energy rechargeable metallic lithium batteries, Nat. Commun. 4 (2013) 1481–1489.
[17] F. Ding, W. Xu, G.L. Graff, J. Zhang, M.L. Sushko, X.L. Chen, Y.Y. Shao, M.H. Engelhard, Z.M. Nie, J. Xiao, X.J. Liu, P.V. Sushko, J. Liu, J.-G. Zhang, Dendrite-free lithium deposition via self-healing electrostatic shield mechanism, J. Am. Chem. Soc. 135 (2013) 4450–4456.
[18] Y. Zhang, J. Qian, W. Xu, S.M. Russell, X. Chen, E. Nasybulin, P. Bhattacharya, M.H. Engelhard, D. Mei, R. Cao, F. Ding, A.V. Cresce, K. Xu, J.-G. Zhang, Dendrite-free lithium deposition with self-aligned nanorod structure, Nano Lett. 14 (2014) 6889–6896.
[19] H. Lee, D.J. Lee, Y.-J. Kim, J.-K. Park, H.-T. Kim, A simple composite protective layer coating that enhances the cycling stability of lithium metal batteries, J. Power Sources 284 (2015) 103–108.
[20] K. Yan, H.-W. Lee, T. Gao, G. Zheng, H. Yao, H. Wang, Z. Lu, Y. Zhou, Z. Liang, Z. Liu, S. Chu, Y. Cui, Ultrathin two-dimensional atomic crystals as stable interfacial layer for improvement of lithium metal anode, Nano Lett. 14 (2014) 6016–6022.
[21] D. Lv, Y. Shao, T. Lozano, W.D. Bennett, G.L. Graff, B. Polzin, J. Zhang, M.H. Engelhard, N.T. Saenz, W.A. Henderson, P. Bhattacharya, J. Liu, J. Xiao, Failure mechanism for fast-charged lithium metal batteries with liquid electrolytes, Adv. Energy Mater. 5 (2015).
[22] H. Yoon, P.C. Howlett, A.S. Best, M. Forsyth, D.R. MacFarlane, Fast charge/discharge of Li metal batteries using an ionic liquid electrolyte, J. Electrochem. Soc. 160 (2013) A1629–A1637.
[23] R. Miao, J. Yang, X. Feng, H. Jia, J. Wang, Y. Nuli, Novel dual-salts electrolyte solution for dendrite-free lithium-metal based rechargeable batteries with high cycle reversibility, J. Power Sources 271 (2014) 291–297.
[24] K. Xu, Nonaqueous liquid electrolytes for lithium-based rechargeable batteries, Chem. Rev. 104 (2004) 4303–4418.
[25] L.A. Dominey, V.R. Koch, T. Blakley, Thermally stable lithium salts for polymer electrolytes, Electrochim. Acta 37 (1992) 1551–1554.
[26] K. Matsumoto, K. Inoue, K. Nakahara, R. Yuge, T. Noguchi, K. Utsugi, Suppression of aluminum corrosion by using high concentration LiTFSI electrolyte, J. Power Sources 231 (2013) 234–238.
[27] H. Yang, K. Kwon, T.M. Devine, J.W. Evans, Aluminum corrosion in lithium batteries an investigation using the electrochemical quartz crystal microbalance, J. Electrochem. Soc. 147 (2000) 4399–4407.
[28] M. Morita, T. Shibata, N. Yoshimoto, M. Ishikawa, Anodic behavior of aluminum current collector in LiTFSI solutions with different solvent compositions, J. Power Sources 119–121 (2003) 784–788.
[29] X. Chen, W. Xu, M.H. Engelhard, J. Zheng, Y. Zhang, F. Ding, J. Qian, J.-G. Zhang, Mixed salts of LiTFSI and LiBOB for stable $LiFePO_4$-based batteries at elevated temperatures, J. Mater. Chem. A 2 (2014) 2346–2352.
[30] H. Xiang, D. Mei, P. Yan, P. Bhattacharya, S.D. Burton, A. von Wald Cresce, R. Cao, M.H. Engelhard, M.E. Bowden, Z. Zhu, B.J. Polzin, C.-M. Wang, K. Xu, J.-G. Zhang, W. Xu, The role of cesium cation in controlling interphasial chemistry on graphite anode in propylene carbonate-rich electrolytes, ACS Appl. Mater. Interfaces 7 (2015) 20687–20695.
[31] M. J. Frisch, G. W. Trucks, H. B. Schlegel, G. E. Scuseria, M. A. Robb, J. R. Cheeseman, G. Scalmani, V. Barone, B. Mennucci, G. A. Petersson, H. Nakatsuji, M. Caricato, X. Li, H. P. Hratchian, A. F. Izmaylov, J. Bloino, G. Zheng, J. L. Sonnenberg, M. Hada, M. Ehara, K. Toyota, R. Fukuda, J. Hasegawa, M. Ishida, T. Nakajima, Y. Honda, O. Kitao, H. Nakai, T. Vreven, J. A. Montgomery Jr., J. E. Peralta, F. Ogliaro, M. J. Bearpark, J. Heyd, E. N. Brothers, K. N. Kudin, V. N. Staroverov, R. Kobayashi, J. Normand, K. Raghavachari, A. P. Rendell, J. C. Burant, S. S. Iyengar, J. Tomasi, M. Cossi, N. Rega, N. J. Millam, M. Klene, J. E. Knox, J. B. Cross, V. Bakken, C. Adamo, J. Jaramillo, R. Gomperts, R. E. Stratmann, O. Yazyev, A. J. Austin, R. Cammi, C. Pomelli, J. W. Ochterski, R. L. Martin, K. Morokuma, V. G. Zakrzewski, G. A. Voth, P. Salvador, J. J. Dannenberg, S. Dapprich, A. D. Daniels, Ö. Farkas, J. B. Foresman, J. V. Ortiz, J. Cioslowski, D. J. Fox; Gaussian, Inc.: Wallingford, CT, USA, 2009.
[32] S.F. Boys, F. Bernardi, The calculation of small molecular interactions by the differences of separate total energies. Some procedures with reduced errors, Mol. Phys. 19 (1970) 553–566.
[33] C. Lee, W. Yang, R.G. Parr, Development of the Colle-Salvetti correlation-energy formula into a functional of the electron density, Phys. Rev. B 37 (1988) 785–789.
[34] K. Xu, S.S. Zhang, U. Lee, J.L. Allen, T.R. Jow, LiBOB: is it an alternative salt for lithium ion chemistry? J. Power Sources 146 (2005) 79–85.
[35] J.Y. Huang, X.J. Liu, X.L. Kang, Z.X. Yu, T.T. Xu, W.H. Qiu, Study on γ-butyrolactone for LiBOB-based electrolytes, J. Power Sources 189 (2009) 458–461.
[36] R.-S. Kühnel, A. Balducci, Comparison of the anodic behavior of aluminum current collectors in imide-based ionic liquids and consequences on the stability of high voltage supercapacitors, J. Power Sources 249 (2014) 163–171.
[37] K. Xu, U. Lee, S. Zhang, M. Wood, T.R. Jow, Chemical analysis of graphite/electrolyte interface formed in LiBOB-based electrolytes, Electrochem. Solid State Lett. 6 (7) (2003) A144–A148.
[38] K. Xu, S.S. Zhang, T.R. Jow, Formation of the graphite/electrolyte interface by lithium *bis*(oxalato)borate, Electrochem. Solid State Lett. 6 (6) (2003) A117–A120.
[39] R. Fong, U.v. Sachen, J.R. Dahn, Studies of lithium intercalation into carbons using nonaqueous electrochemical cells, J. Electrochem. Soc. 137 (7) (1990) 2009–2013.
[40] D. Aurbach, Nonaqueous Electrochemistry, CRC Press, New York, 1999, p. 307.